Published in final edited form as:
JACC Cardiovasc Interv. 2009 November ; 2(11): 1035–1046. doi:10.1016/j.jcin.2009.06.019.

Intracoronary Optical Coherence Tomography: A Comprehensive Review:

Clinical and Research Applications

Hiram G. Bezerra, MD, PHD[*], **Marco A. Costa, MD, PHD**[*], **Giulio Guagliumi, MD**[‡], **Andrew M. Rollins, PHD**[†], and **Daniel I. Simon, MD**[*]

[*]Harrington-McLaughlin Heart & Vascular Institute, University Hospitals Case Medical Center, Cleveland, Ohio

[†]Department of Biomedical Engineering, Case Western Reserve University School of Medicine, Cleveland, Ohio

[‡]Cardiovascular Department Ospedali Riuniti di Bergamo, Bergamo, Italy

Abstract

Cardiovascular optical coherence tomography (OCT) is a catheter-based invasive imaging system. Using light rather than ultrasound, OCT produces high-resolution in vivo images of coronary arteries and deployed stents. This comprehensive review will assist practicing interventional cardiologists in understanding the technical aspects of OCT based upon the physics of light and will also highlight the emerging research and clinical applications of OCT. Semi-automated imaging analyses of OCT systems permit accurate measurements of luminal architecture and provide insights regarding stent apposition, overlap, neointimal thickening, and, in the case of bioabsorbable stents, information regarding the time course of stent dissolution. The advantages and limitations of this new imaging modality will be discussed with emphasis on key physical and technical aspects of intracoronary image acquisition, current applications, definitions, pitfalls, and future directions.

Keywords

optical coherence tomography; coronary; stent; atherosclerosis

Concepts in Biophotonics

The fundamental principles of optical coherence tomography (OCT) evolved from optical 1-dimensional low-coherence reflectometry, which uses a Michelson interferometer and a broadband light source. In 1991, the addition of transverse scanning (B-scan), enabled 2-dimensional imaging of the retina (1). This technique was named OCT by James Fujimoto and rapidly expanded to numerous biomedical and clinical applications. Intravascular OCT

Reprint requests and correspondence: Dr. Marco A. Costa, Division of Cardiology, Heart & Vascular Institute, University Hospitals, Case Western Reserve University, 11100 Euclid Avenue, Lakeside 3001, Cleveland, Ohio 44106-5038. marco.costa@uhhospitals.org.

requires a single fiberoptic wire that both emits light and records the reflection while simultaneously rotating and being pulled back along the artery.

The coronary OCT light source uses a bandwidth in the near-infrared spectrum with central wavelengths ranging from 1,250 to 1,350 nm. Although longer wavelengths provide deeper tissue penetration, the optimal choice of wavelength in an arterial vessel is also defined by tissue absorption characteristics and the refractive index of the interface between the catheter and vessel wall. Current intravascular OCT systems use a central wavelength of approximately 1,300 nm. Using this wavelength the tissue penetration is limited to 1 to 3 mm as compared with 4 to 8 mm achieved by intravascular ultrasound (IVUS), with the exception of calcified lesions in which sound has a limited penetration.

The image is formed by the backscattering of light from the vessel wall or the time it takes for emitted light to travel between the target tissue and back to the lens, producing an “echo time delay” with a measurable signal intensity or “magnitude.” Multiple axial scans (A-lines) are continuously acquired as the imagewire rotates and a full revolution creates a complete cross section of the vessel.

It is important to note that the speed of light (3×10^8 m/s) is much faster than that of sound (1,500 m/s), and, therefore, interferometry techniques are necessary to measure the backscattered signal since a direct quantification cannot be achieved on such a time scale. The interferometer uses a fiberoptic coupler similar to a beam splitter, which directs one-half of the beam to the tissue and the other one-half to the reference arm. The reference arm of a time-domain optical coherence tomography (TD-OCT) system consists of a mirror moving at calibrated distances to produce known echo delays. The reflected signal returning from the tissue and reference arms are recombined in the fiber-coupler, and their interference fringes are detected by a photodetector. The general scheme of an intravascular OCT system is shown in Figure 1.

The axial resolution, determined by the light wavelength, ranges from 12 to 18 μm, compared with 150 to 200 μm for IVUS. The lateral resolution and depth of focus are decoupled from the axial resolution and defined by the spot size focused by the lens in the sample arm. The lateral resolution in catheter-based OCT is typically 20 to 90 μm as compared with 150 to 300 μm for IVUS. For faster image acquisition, the ideal choice is to accelerate the acquisition time of each A-line. This process generates faster cross-sectional imaging, in turn resulting in a higher number of frames per second, which ultimately yields a faster pullback. However, further improvement in speed for time-domain OCT systems is physically limited by generating a fast optical delay in the reference arm and the tradeoff between the imaging speed and sensitivity. Newer-generations of intravascular OCT systems circumvent this limitation by using a fixed mirror with a variable frequency light source or “swept-laser.” This method, termed frequency or Fourier-domain optical coherence tomography (FD-OCT), allows the simultaneous detection of reflections from all echo time delays, making the system significantly faster (2). There are 2 types of FD-OCT systems that differ in their method of data extraction from the interferometer: optical frequency domain imaging also known as swept-source OCT, or a spectral domain OCT. The specific features of each system of transformation are outside the scope of this article. A diagram of

the main components of the TD-OCT and FD-OCT systems are shown in Figure 1 and their features contrasted in Table 1.

Commercial OCT Systems

The first commercially available OCT system was the LightLab M2 TD-OCT Imaging System (LightLab, Westford, Massachusetts). Recently an FD-OCT system (C7 XR, LightLab) has become commercially available in the European Union, Asia, and South America. In the M2/M3 systems, images are recorded by an ImageWire (LightLab), a general purpose, single-mode, fiberoptic wire that rotates inside a fluid-filled polymer tube. A micro lens assembly at the distal end is ~1 mm in length and 125 μm in diameter (similar to the fiber itself). This assembly focuses and reflects the light beam at ~80° from the fiber's axis to allow circumferential imaging of the vessel. The wire is attached to an automated pullback engine integrated with the console. The external diameter of the imagewire is 0.019 inches and is fused to a short segment of a standard 0.014-inch guidewire at the distal end. An over-the-wire low-pressure occlusion balloon catheter (Helios, Goodman, Nagoya, Japan) with distal flush ports is used to infuse saline or Ringer's Lactate at approximately 0.5 ml/s to selectively displace blood during imaging acquisition. Blood must be completely removed, as any amount of residual red blood cells causes significant signal attenuation. Because of safety concerns, the occlusion time is limited by the manufacturer to 30 s. Similar balloon occlusion techniques are used with angioscopy. The new FD-OCT systems can acquire 100 frames/s, reaching pullback speeds up to 20 mm/s with the potential to scan 4- to 6-cm length epicardial coronary vessels in <5 s (3,4). Accelerated pullback speeds permit the use of a single, high rate (~4 cc/s) bolus injection of contrast to produce a blood-free environment, thereby eliminating the need for balloon occlusion (3,4) (Table 1). The Lightlab FD-OCT system is equipped with a tunable laser light source with sweep range of 1,250 to 1,370 nm. The optical fiber is encapsulated within a rotating torque wire built in a rapid exchange 2.6-F catheter compatible with 6-F guides. This system has been already tested in humans in Europe and Japan, and is currently under Food and Drug Administration evaluation. Terumo (Terumo Corporation, Tokyo, Japan) is developing an FD-OCT system, which has a 2.4-F shaft. Volcano (Volcano Corporation, Rancho Cordova, California) is the third FD-OCT system under development with a rapid-exchange nitinol hybrid drive shaft (5).

OCT Imaging Acquisition Technique

Despite its guidewire-like profile, the OCT ImageWire (Lightlab TD-OCT) is not designed to be advanced into the coronary artery as a stand-alone device. Rather, the imagewire is inserted using an over-the-wire balloon catheter (Helios). The Helios balloon has a maximum external diameter of 1.5 mm and is compatible with large 6-F guiding catheters (0.071-inch inner diameter). It is advanced distally to the segment of interest over a conventional angioplasty guidewire (0.014-inch). The guidewire is then exchanged with the OCT ImageWire, and the occlusion balloon is pulled back and repositioned in a healthy proximal segment. The balloon is highly compliant and is inflated at minimal pressure that allows totally clean imaging from blood, usually between 0.4 to 0.7 atm with a dedicated inflator. A contrast injector pump with a warming cuff is set at 0.5 cc/s infusion, which can

be increased to up to 1.0 cc/s until blood is completely cleared. The solution is injected through the end-hole distal port of the occlusion balloon catheter and should start several seconds before balloon occlusion. The pullback speed can be adjusted from 0.5 to 3.0 mm/s, and the entire imagewire is pulled from distal to proximal along the coronary artery. In the next-generation FD-OCT systems, imaging can be performed without balloon occlusion. The pullback speed can reach up to 20 to 40 mm/s and is performed during contrast injection (~4 cc/s) to assure complete blood clearance. Imaging of 4 to 6 cm of coronary artery segments can be achieved with <15 cc of contrast per pullback. For nonocclusion techniques, iodinated contrast media is preferred over saline or Ringer's lactate because of the advantage of high viscosity solutions in completely removing blood.

Operators should be aware of the vessel size range suitable for OCT imaging, particularly with the first generation devices, ideally between 2.0 to 3.75 mm in diameter. The upper limit is restricted by the scan diameter (field of view) and fold-over artifact (specific to FD-OCT systems), addressed later. In fact, "out-of-screen" loss of image represents the most common technical exclusion of frame analysis in the clinical trials examined in our core laboratory. The field of view was significantly enlarged in the new FD-OCT system (Table 1). The need for a proximally placed balloon in conventional TD-OCT imaging limits its ability to evaluate ostial and highly proximal disease in the coronary arteries since inflation of the Helios balloon in an unprotected left main or diseased segment should not be performed. Other potential sources of image distortion include excessive vessel tortuosity and the presence of exuberant collateral flow. Studies comparing OCT versus IVUS suggest that TD-OCT is safe and can be performed with success rates at least comparable with IVUS (6 – 8). Some transient events, such as chest discomfort and ST-T changes, were observed during imaging procedures with OCT or IVUS. Neither hemodynamic instability nor ventricular tachyarrhythmia was observed (7). The feasibility and safety of the larger catheter-based FD-OCT systems remains to be established in future trials.

Pitfalls in imaging post-processing and interpretation Z-offset

Imagewires have minute differences in their optic path lengths. The Z-offset is a manually adjustable image calibration, which is critical for accurate measurements. In the current LightLabs TD-OCT system, the catheter diameter acts as a reference for optimal Z-offset determination within an image frame. The 4 marks or fiduciaries should align to fit the outer surface of the catheter. If the catheter is not well visualized, calibration is performed in a frame where the catheter is in contact with the vascular surface by adjusting the fiduciaries to align the vessel wall. The operator should monitor these patterns throughout the entire pullback since additional adjustments may be necessary. The majority of corrections are typically made in the first 10 mm of the pullback image. In next-generation FD-OCT catheters, a semitransparent catheter around the optic fiber is more suitable for direct calibration. We have observed that a 1% change in the magnitude of the ideal Z-offset can result in a 12% to 14% error in area measurements. Small changes in magnitude can also amplify contour distortion, which may result in misinterpretation of the image.

Artifacts

Some OCT artifacts are common to both OCT and IVUS, and others are unique to OCT imaging systems. Most of these artifacts will not substantially compromise clinical interpretation of the image, if restricted to few noncontinuous frames, but may render imprecise assessment of plaque characteristics or measurements (Fig. 2).

1. *Residual blood* attenuates the OCT light beam and may defocus the beam if red cell density is high. This will reduce brightness of the vessel wall, especially at large radial distances from the ImageWire. If the lumen surface is still clearly defined, the presence of diluted blood does not appear to affect area measurements. Care should be taken to avoid mistakenly labeling residual blood artifact as thrombus or some other specific intra-vascular finding.
2. *Nonuniform rotational distortion* is the result of variation in the rotational speed of the spinning optical fiber. It is usually produced by vessel tortuosity or by an imperfection in the torque wire or sheath interfering with smooth rotation of the optical fiber, which can result in focal image loss or shape distortion. Fortunately, this seems to occur less frequently than in IVUS imaging, perhaps as a result of the smaller profile and simplified rotational mechanics of OCT wires.
3. *Sew-up artifact* is the result of rapid artery or imaging wire movement in 1 frame's imaging formation, leading to single point misalignment of the lumen border.
4. *Saturation artifact* occurs when light reflected from a highly specular surface (usually stent struts) produces signals with amplitudes that exceed the dynamic range of the data acquisition system (Fig. 2). This should be kept in mind when defining the stent surface. We measured the average "normal" blooming of a stainless steel stent from 2,250 struts in 471 cross-sectional OCT images. The mean measured thickness was 37 ± 8 μm (9). These values are important particularly for malapposition quantification since the blooming thickness value needs to be considered in addition to stent and polymer thickness.
5. *Fold-over artifact* is more specific to the new generation of FD-OCT. It is the consequence of the "phase wrapping" or "alias" along the Fourier transformation when structure signals are reflected from outside the system's field of view. Typical examples are side branch and large vessels.
6. *Bubble artifact* occurs when small gas bubbles are formed in the silicon lubricant used to reduce friction between the sheath and the revolving optic fiber in TD-OCT systems. It can attenuate the signal along a region of the vessel wall, and images with this artifact are not suitable for tissue characterization.
7. *Artifacts related to eccentric wire position*. Eccentricity of the imagewire in the vessel lumen can influence many aspects of the image interpretation. This phenomenon is likely secondary to imaging sweep speed, and is more pronounced with an eccentric imagewire position, leading to longer distance between each A-line and consequently decreasing the lateral resolution, and has been dubbed the "merry-go-round" effect (Fig. 3). A byproduct of rotational scanning, the reflection from metallic stent struts align toward the imaging wire, akin to sunflowers

aligning to the sun or a “sunflower” effect. This effect is pronounced with eccentric wire position, as it can display strut reflections almost perpendicular to the lumen surface in oblique regions from the wire. This may have important future implications in the serial assessment of strut length, particularly when evaluating the degradation of bioabsorbable stents.

Clinical Applications

Diagnostic assessment of coronary atherosclerosis

Acknowledging the lack of prospective studies and appropriate animal models to define vulnerable plaque (i.e., rupture-prone), our current understanding of plaque biology suggests that ~80% of clinically evident plaque rupture originates within an inflamed thin-capped fibroatheroma (10). Plaques containing calcium nodules are associated with ~10% of clinical events, and plaque that does not fall into either category is associated with ~20% of clinical atherothrombosis. Superficial plaque erosion may comprise a portion of these events, especially in women and diabetic patients. Because plaque erosion does not have a typical cellular or anatomical signature, it is currently difficult to prospectively identify those plaques at risk by existing imaging methods. Clinical plaque erosion has been reported by OCT in a similar frequency to pathologic studies (11,12).

Thin-capped fibroatheromas are characterized by 3 essential components: a lipid core, inflammatory cell cap infiltration, and a thin fibrous cap. While OCT does not currently have the depth to quantify large lipid cores, its high resolution allows precise visualization and quantification of the thin fibrous cap (11,13).

FIBROUS CAP—While seminal post-mortem investigations have suggested that a cap thickness <65 μm (14) is associated with plaque rupture, OCT has demonstrated that patterns of plaque rupture and fibrous cap thickness vary widely. Illustrating this heterogeneity, OCT showed 93% of the culprit plaques in patients presenting with acute myocardial infarction triggered by exertion had rupture at the shoulder, where the average cap thickness was 90 μm. In contrast, 57% of acute myocardial infarction patients who experienced symptoms at rest had plaque rupture in the shoulder with an average cap thickness of 50 μm (15). OCT provides the potential for fibrous cap plaque measurement (Fig. 4) and was recently used to demonstrate a significant increase in cap thickness in patients taking a statin versus a control group (16).

INFLAMMATION—The large size of macrophages and their high lipid content yield strong optical signals (17–19). Clusters of macrophages can appear as bright spots along the fibrous cap. However, data supporting OCT’s capability to quantify macrophages used raw (linear) OCT data from early generation systems (18). The accuracy and validation of current clinical OCT systems for the evaluation of macrophages remains to be demonstrated.

LIPID NECROTIC CORE—The lipid/fibrous tissue interface causes a surrounding border of high superficial backscattering. However, light does not penetrate deeply into the necrotic core, and is further absorbed by the lipid tissue providing a subsequent region of low or no

signal casting the vascular wall beyond in shadow. This makes the extent of the lipid pool or vascular remodeling difficult to quantify.

CALCIUM NODULES—In contrast to ultrasound, light penetrates calcium and OCT depicts calcium with well-defined boundaries (Fig. 5). One OCT study has reported a sensitivity of 96% and specificity of 97% to detect calcified nodules (13).

THROMBUS—Previous studies have suggested that it is possible to identify thrombus by OCT and even discriminate between red and white thrombus, as confirmed by histopathologic correlation (20) (Table 2). The sensitivity of OCT to detect thrombus appears to possibly be higher than that of ultrasound (11,21), but these studies were conducted in a selected population with a high pre-test probability of thrombus. In our experience of >500 detailed OCT coronary stent analyses, the discrimination of thrombus from other potentially abnormal intraluminal images can be ambiguous, particularly when these analyses are blinded. Overall, OCT may possess diagnostic advantages compared with both IVUS and angioscopy in the assessment of culprit lesions. Plaque rupture was identifiable in 73% of OCT images compared with 40% and 47%, respectively, for IVUS and angioscopy; moreover, plaque erosion was almost exclusively identified by OCT (23%) in a cohort of patients with acute myocardial infarction (11). The same study reported thrombus identification in all cases by OCT and angioscopy, but only in 33% of IVUS images.

OCT-guided coronary intervention

Assessment of lumen geometry remains the cornerstone of intravascular imaging criteria to evaluate disease severity and guide interventional procedures. Minimal lumen area, percentage lumen obstruction, percent neointimal hyperplasia (NIH), stent apposition, stent expansion, minimal stent cross section area, lumen gain, late lumen loss, and restenosis are all based on the evaluation of the lumen-vessel/stent interface (22–30). OCT images provide a clear depiction of the boundaries between lumen and vessel. OCT's ability to penetrate and delineate calcium in the vessel wall makes it well suited to guide complex interventional strategies in vessels with superficial calcification (Fig. 6D). It is important to note that IVUS-guided vessel dimensions and criteria for percutaneous coronary intervention may vary between different imaging modalities or even different quantification software (31).

We and others have demonstrated the higher sensitivity of OCT compared with IVUS for malapposed strut assessment (32,33). Plaque protrusion and stent-edge dissection are other common intervention-related parameters readily visible on OCT images, although their clinical impact remains to be assessed.

Research Applications of Intravascular OCT

End point for clinical trials

Stent-strut coverage and apposition have been linked to the risk of stent thrombosis (34,35), and recent DES clinical trials, such as the ODESSA (OCT for DES SAfety) study, have selected these variables as their primary end point (36). Histologic studies have revealed that IVUS does not have adequate resolution to detect the thinnest layers of tissue coverage (37),

and the perception that lack of NIH by IVUS is synonymous to an uncovered strut needs to be reconsidered. In a sub-analysis of the ODESSA trial, we identified 20 of 250 stented segments with no detectable NIH by IVUS, but had neointimal coverage ranging from 67% to 100% by OCT (38). In contrast to the relatively homogenous lack of NIH detected by IVUS, OCT revealed a highly heterogeneous response to DES, which varied even within the same cross-sectional image.

Strut-level analysis

Our current method of *strut-level analysis* stratifies struts into 4 main categories: covered-embedded, covered-protruding (into the lumen but covered), uncovered-apposed, and malapposed. A semiautomated stent contour algorithm applies 360 radial chords for detailed quantification of NIH thickness at every degree of the cross section (Fig. 7). The continuous sampling obtained by OCT also represents an advantage over standard histopathology, which evaluates cross sections in intervals of 2 to 3 mm (39). Taking advantage of such OCT features, one may be able to gather enough information from a relatively small patient cohort to guide drug and device industry before embarking on large population trials.

Our understanding of DES healing in patients with ST-segment elevation myocardial infarction was restricted to post-mortem data (39). A high-rate (49%) of uncovered struts was observed in previous pathology studies, but the limited number of specimens (n = 25) and inherent selection bias of such studies precluded any definitive conclusions. The OCT substudy of the HORIZONS (Harmonizing Outcomes with Revascularization and Stents in AMI) trial (40) evaluated 117 patients (199 stents) in a prospective, randomized and blinded manner. Stent struts were analyzed at every 0.3 mm at 13-month post-stenting and revealed a higher percentage of strut coverage in both bare-metal stents and drug-eluting stents (98.9% vs. 94.3%, $p < 0.001$) compared with autopsy studies (9).

An important limitation of OCT is the limited precision in discriminating the different kinds of tissue coverage of stents (i.e., endothelium, smooth muscle cells, extracellular matrix). Future studies using histopathologic correlations are needed to define “normal” and “abnormal” stent healing and vessel wall passivation. Importantly, the spatial resolution of current OCT systems is insufficient to detect cell layer thickness <20 μm on the stent surface, thereby precluding a precise distinction between “true lack of cellular coverage” versus 3 to 5 cell layer coverage of stent struts. On a research basis, OCT is well suited for studying vascular healing over time. In the ongoing OCTAXUS (OCT Taxus) study, OCT imaging is being performed at 3-and 9-month intervals after stent deployment. Serial studies or observational studies at defined time points may also be helpful in clarifying the role of adjunctive pharmacology in the context of vascular healing (e.g., the intensity and duration of antiplatelet therapy).

The Future Outlook

The future of OCT will include advancements in anatomical and functional assessment of lesions for the interventional cardiologist.

Anatomical assessment

An advanced *edge detection* algorithm that enables automated stent strut identification is already available in the research laboratory and is likely to appear in the cathlab in the near future. A similar concept is also being applied to help facilitate tissue characterization (e.g., sharp edges of calcium can be differentiated from diffuse lipid appearance) (Table 2) (Fig. 5). *Texture analysis* of OCT images may also help facilitate tissue characterization, (e.g., "fractal analysis" uses a computational method of calculating the extent of entropy or randomness found in the tissue image). *Polarization* takes advantage of the random scattering found in some tissues and reproducible birefringence found in other highly organized tissues (a property of collagen-rich tissue). Perhaps this may serve as a future index of plaque stability since this organized fibrous tissue seems to be protective. *Ultra-high resolution OCT*, as the name suggests, aims to resolve images to <10 m*μ*. Strategies to accomplish this include ultra-broadband light sources, lower central wavelengths (41), femtosecond lasers (42– 45), and multiple superluminescent diodes.

Functional assessment

Contrast enhanced and molecular OCT is an evolving field based on the development and use of nanoparticles, microspheres, and absorbing dyes to increase the local properties of scattering and absorption of light in targeted tissues. Detection of *Doppler*-like signals using a TD-OCT ImageWire may permit a biophotonic version of the flow wire, thereby allowing integration of physiology and anatomical assessment using a single device.

Conclusions

OCT enhances imaging resolution (Fig. 8) that may permit the evaluation of clinical (e.g., luminal measurements during PCI) and research (e.g., fibrous cap thickness and strut level analysis) parameters for the interventional cardiologist. The versatility of the physical properties of light position OCT as an imaging modality could be useful for improving our understanding of the vascular biology of atherothrombosis and assisting in our performance of PCI procedures. However, routine clinical use of OCT will require further clinical trials to validate the technology, establish standard definitions/measurements, and to test its safety and utility in improving clinical outcomes.

Acknowledgments

Dr. Bezerra received research grants and consulting honoraria from Lightlab. Dr. Costa received research grants and consulting honoraria from Lightlab and Cordis/Johnson & Johnson. Dr. Guagliumi received research grants from Medtronic Vascular, Lightlab, and Boston Scientific. Dr. Simon received research grants from Medtronic Vascular and Cordis/Johnson & Johnson.

Abbreviations and Acronyms

A-line	axial line (scan)
FD-OCT	frequency or Fourier-domain optical coherence tomography
IEL/EEL	internal elastic lamina/external elastic lamina

IVUS	intravascular ultrasound
NIH	neointimal hyperplasia
OCT	optical coherence tomography
TD-OCT	time-domain optical coherence tomography

References

1. Huang D, Swanson EA, Lin CP, et al. Optical coherence tomography. Science. 1991; 254:1178–81. [PubMed: 1957169]
2. Chinn SR, Swanson EA, Fujimoto JG. Optical coherence tomography using a frequency-tunable optical source. Opt Lett. 1997; 22:340–2. [PubMed: 18183195]
3. Tearney GJ, Waxman S, Shishkov M, et al. Three-dimensional coronary artery microscopy by intracoronary optical frequency domain imaging. J Am Coll Cardiol Img. 2008; 1:752–61.
4. Barlis P, Schmitt JM. Current and future developments in intracoronary optical coherence tomography imaging. EuroIntervention. 2009; 4:529–33. [PubMed: 19284077]
5. Guagliumi G, Sirbu V. Optical coherence tomography: high resolution intravascular imaging to evaluate vascular healing after coronary stenting. Catheter Cardiovasc Interv. 2008; 72:237–47. [PubMed: 18655155]
6. Serruys PW, Ormiston JA, Onuma Y, et al. A bioabsorbable everolimus-eluting coronary stent system (ABSORB): 2-year outcomes and results from multiple imaging methods. Lancet. 2009; 373:897–910. [PubMed: 19286089]
7. Yamaguchi T, Terashima M, Akasaka T, et al. Safety and feasibility of an intravascular optical coherence tomography image wire system in the clinical setting. Am J Cardiol. 2008; 101:562–7. [PubMed: 18307999]
8. Kubo T, Imanishi T, Kitabata H, et al. Comparison of vascular response after sirolimus-eluting stent implantation between patients with unstable and stable angina pectoris: a serial optical coherence tomography study. J Am Coll Cardiol Img. 2008; 1:475–84.
9. Guagliumi, G.; Sirbu, V.; Costa, M., et al. Long-term Strut Coverage of Paclitaxel Eluting Stents Compared to Bare-Metal Stents Implanted During Primary PCI in Acute Myocardial Infarction. A Prospective, Randomized, Controlled Study Performed with Optical Coherence Tomography. HORIZONS-OCT. Paper presented at: Late Breaking Trials, American Heart Association Annual Meeting; November 15, 2008; New Orleans, LA.
10. Schaar, JA.; Muller, JE.; Falk, E., et al. Terminology for high-risk and vulnerable coronary artery plaques. Eur Heart J; Report of a meeting on the vulnerable plaque; June 17 and 18, 2003; Santorini, Greece. 2004. p. 1077-82.
11. Kubo T, Imanishi T, Takarada S, et al. Assessment of culprit lesion morphology in acute myocardial infarction: ability of optical coherence tomography compared with intravascular ultrasound and coronary angioscopy. J Am Coll Cardiol. 2007; 50:933–9. [PubMed: 17765119]
12. Farb A, Burke AP, Tang AL, et al. Coronary plaque erosion without rupture into a lipid core. A frequent cause of coronary thrombosis in sudden coronary death. Circulation. 1996; 93:1354–63. [PubMed: 8641024]
13. Yabushita H, Bouma BE, Houser SL, et al. Characterization of human atherosclerosis by optical coherence tomography. Circulation. 2002; 106:1640–5. [PubMed: 12270856]
14. Burke AP, Farb A, Malcom GT, Liang YH, Smialek J, Virmani R. Coronary risk factors and plaque morphology in men with coronary disease who died suddenly. N Engl J Med. 1997; 336:1276–82. [PubMed: 9113930]
15. Tanaka A, Imanishi T, Kitabata H, et al. Distribution and frequency of thin-capped fibroatheromas and ruptured plaques in the entire culprit coronary artery in patients with acute coronary syndrome as determined by optical coherence tomography. Am J Cardiol. 2008; 102:975–9. [PubMed: 18929696]

16. Takarada S, Imanishi T, Kubo T, et al. Effect of statin therapy on coronary fibrous-cap thickness in patients with acute coronary syndrome: assessment by optical coherence tomography study. Atherosclerosis. 2009; 202:491–7. [PubMed: 18572175]

17. MacNeill BD, Jang IK, Bouma BE, et al. Focal and multi-focal plaque macrophage distributions in patients with acute and stable presentations of coronary artery disease. J Am Coll Cardiol. 2004; 44:972–9. [PubMed: 15337206]

18. Tearney GJ, Jang IK, Bouma BE. Optical coherence tomography for imaging the vulnerable plaque. J Biomed Opt. 2006; 11:021002. [PubMed: 16674177]

19. Raffel OC, Tearney GJ, Gauthier DD, Halpern EF, Bouma BE, Jang IK. Relationship between a systemic inflammatory marker, plaque inflammation, and plaque characteristics determined by intravascular optical coherence tomography. Arterioscler Thromb Vasc Biol. 2007; 27:1820–7. [PubMed: 17541021]

20. Kume T, Akasaka T, Kawamoto T, et al. Assessment of coronary arterial thrombus by optical coherence tomography. Am J Cardiol. 2006; 97:1713–7. [PubMed: 16765119]

21. Tanimoto T, Imanishi T, Tanaka A, et al. Various types of plaque disruption in culprit coronary artery visualized by optical coherence tomography in a patient with unstable angina. Circ J. 2009; 73:187–9. [PubMed: 19001748]

22. Schiele F, Meneveau N, Vuillemenot A, et al. Impact of intravascular ultrasound guidance in stent deployment on 6-month restenosis rate: a multicenter, randomized study comparing two strategies —with and without intravascular ultrasound guidance. RESIST Study Group. REStenosis after Ivus guided STenting. J Am Coll Cardiol. 1998; 32:320–8. [PubMed: 9708456]

23. Mudra H, di Mario C, de Jaegere P, et al. Randomized comparison of coronary stent implantation under ultrasound or angiographic guidance to reduce stent restenosis (OPTICUS study). Circulation. 2001; 104:1343–9. [PubMed: 11560848]

24. Oemrawsingh PV, Mintz GS, Schalij MJ, Zwinderman AH, Jukema JW, van der Wall EE. Intravascular ultrasound guidance improves angiographic and clinical outcome of stent implantation for long coronary artery stenoses: final results of a randomized comparison with angiographic guidance (TULIP study). Circulation. 2003; 107:62–7. [PubMed: 12515744]

25. Serruys PW, Degertekin M, Tanabe K, et al. Intravascular ultrasound findings in the multicenter, randomized, double-blind RAVEL (RAndomized study with the sirolimus-eluting VElocity balloon-expandable stent in the treatment of patients with de novo native coronary artery Lesions) trial. Circulation. 2002; 106:798–803. [PubMed: 12176950]

26. Cook S, Wenaweser P, Togni M, et al. Incomplete stent apposition and very late stent thrombosis after drug-eluting stent implantation. Circulation. 2007; 115:2426–34. [PubMed: 17485593]

27. Windecker S, Meier B. Late coronary stent thrombosis. Circulation. 2007; 116:1952–65. [PubMed: 17965406]

28. Kotani J, Awata M, Nanto S, et al. Incomplete neointimal coverage of sirolimus-eluting stents: angioscopic findings. J Am Coll Cardiol. 2006; 47:2108–11. [PubMed: 16697331]

29. Hong MK, Mintz GS, Lee CW, et al. Late stent malapposition after drug-eluting stent implantation: an intravascular ultrasound analysis with long-term follow-up. Circulation. 2006; 113:414–9. [PubMed: 16432073]

30. Okabe T, Mintz GS, Buch AN, et al. Intravascular ultrasound parameters associated with stent thrombosis after drug-eluting stent deployment. Am J Cardiol. 2007; 100:615–20. [PubMed: 17697816]

31. Hoffmann R, Mintz GS, Popma JJ, et al. Overestimation of acute lumen gain and late lumen loss by quantitative coronary angiography (compared with intravascular ultrasound) in stented lesions. Am J Cardiol. 1997; 80:1277–81. [PubMed: 9388098]

32. Bouma BE, Tearney GJ, Yabushita H, et al. Evaluation of intracoronary stenting by intravascular optical coherence tomography. Heart. 2003; 89:317–20. [PubMed: 12591841]

33. Rosenthal N, Guagliumi G, Sirbu V, et al. Comparison of intravascular ultrasound and optical coherence tomography for the evaluation of stent segment malapposition (abstr). J Am Coll Cardiol. 2009; 53 (Suppl A):A22.

34. Finn AV, Kolodgie FD, Harnek J, et al. Differential response of delayed healing and persistent inflammation at sites of overlapping sirolimus- or paclitaxel-eluting stents. Circulation. 2005; 112:270–8. [PubMed: 15998681]
35. Hassan AK, Bergheanu SC, Stijnen T, et al. Late stent malapposition risk is higher after drug-eluting stent compared with bare-metal stent implantation and associates with late stent thrombosis. Eur Heart J. 2009 Jan 21. E-pub ahead of print.
36. Guagliumi, G.; Musumeci, G.; Sirbu, V., et al. A Prospective, Randomized, Controlled Study Using Optical Coherence Tomography to Evaluate Strut Coverage of Sirolimus-, Paclitaxel-, and Zotarolimus-Eluting Coronary Stents in Long Lesions Requiring Overlapping. Paper presented at: Late Breaking Trials, Transcatheter Cardiovascular Therapeutics Annual Meeting; October 14, 2008; Washington, DC.
37. Sousa JE, Costa MA, Sousa AG, et al. Two-year angiographic and intravascular ultrasound follow-up after implantation of sirolimus-eluting stents in human coronary arteries. Circulation. 2003; 107:381–3. [PubMed: 12551858]
38. Bezerra H, Guagliumi G, Valescchi O, et al. Unraveling the lack of neointimal hyperplasia detected by intravascular ultrasound using optical coherence tomography: lack of spatial resolution or a true biological effect? (abstr). J Am Coll Cardiol. 2009; 53 (Suppl A):90A.
39. Nakazawa G, Finn AV, Joner M, et al. Delayed arterial healing and increased late stent thrombosis at culprit sites after drug-eluting stent placement for acute myocardial infarction patients: an autopsy study. Circulation. 2008; 118:1138–45. [PubMed: 18725485]
40. Guagliumi G, Sirbu V, Costa M, da Costa CA. Long-term strut coverage of paclitaxel eluting stents compared with bare-metal stents implanted during primary PCI in acute myocardial infarction: a prospective, randomized, controlled study performed with optical coherence tomography. HORIZONS-OCT (abstr). Circulation. 2008; 118:2315.
41. Wang H, Fleming CP, Rollins AM. Ultrahigh-resolution optical coherence tomography at 1. 15 um using photonic crystal fiber with no zero-dispersion wavelengths. Opt Express. 2007; 15:3085–92. [PubMed: 19532547]
42. Hartl I, Li XD, Chudoba C, et al. Ultrahigh-resolution optical coherence tomography using continuum generation in an air silica microstructure optical fiber. Opt Lett. 2001; 26:608–10. [PubMed: 18040398]
43. Herz P, Chen Y, Aguirre A, et al. Ultrahigh resolution optical biopsy with endoscopic optical coherence tomography. Opt Express. 2004; 12:3532–42. [PubMed: 19483882]
44. Drexler W. Ultrahigh-resolution optical coherence tomography. J Biomed Opt. 2004; 9:47. [PubMed: 14715057]
45. Wang H, Jenkins MW, Rollins AM. A combined multiple-SLED broadband light source at 1300 nm for high resolution optical coherence tomography. Opt Commun. 2008; 281:1896–900.

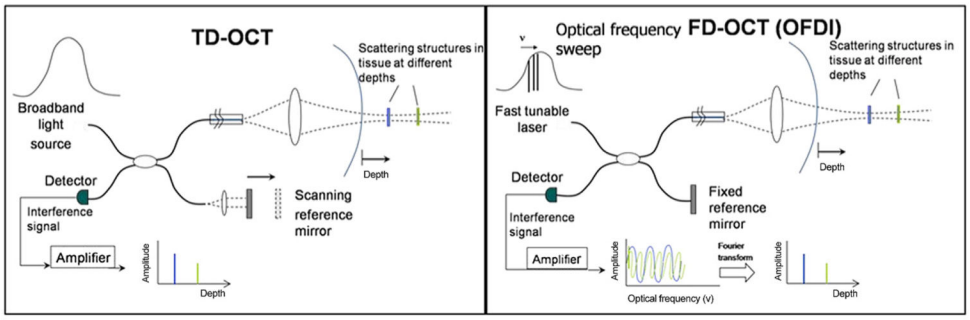

Figure 1. Scheme of TD-OCT and FD-OCT

A schematic representation of time-domain optical coherence tomography (TD-OCT, **left panel**) and frequency or Fourier-domain optical coherence tomography (FD-OCT, **right panel** depicts a subtype of FD-OCT called optical frequency domain imaging [OFDI OCT]). Both systems use a reference arm and an interferometer to detect echo time delays of light. The interferometer uses a beamsplitter, dividing the light into a measurement arm (tissue sample) and a reference arm. The reference arm in TD-OCT is mechanically scanned (by a moving mirror) in order to produce a time-varying time delay. In the FD-OCT, because the light source is frequency swept, the interference of the 2 light beams (tissue and reference) oscillates according to the frequency difference. In both systems the interference of the signal ultimately provides amplitude and frequency data. In the FD-OCT system, all echo delays are acquired simultaneously enabling significant increases in the speed of image acquisition.

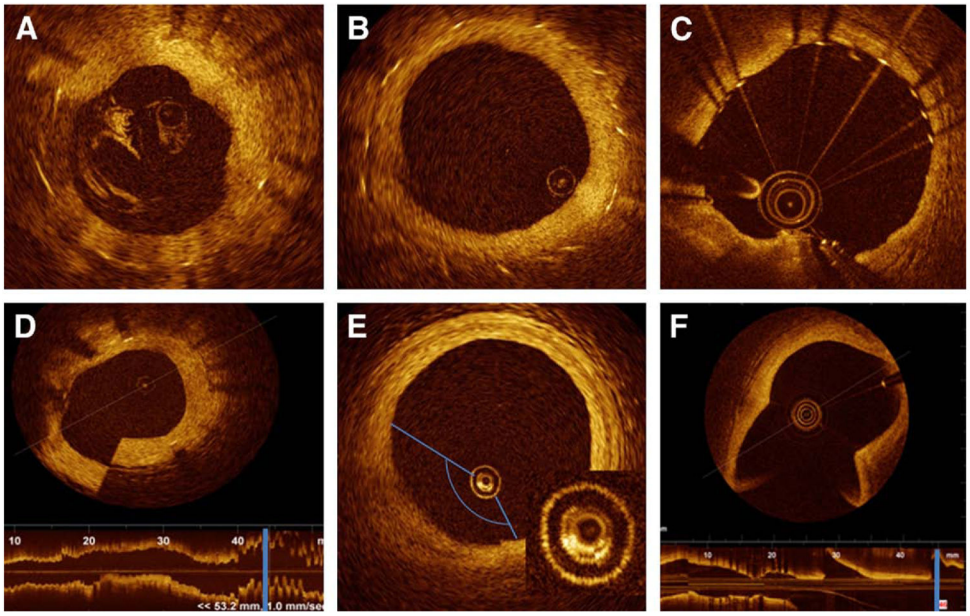

Figure 2. Most Frequent Artifacts

Cross-sectional image of the human coronary artery. Most frequently observed artifacts: **(A)** incomplete blood displacement, resulting in light attenuation. **(B)** Eccentric image wire can distort stent reflection orientation, the struts align toward the imaging wire “sunflower effect” and are elongated “merry-go-round.” **(C)** Saturation artifact, some scan lines have a streaked appearance. **(D)** Sew-up artifact: result of rapid wire or vessel movement along 1 frame formation, resulting in misalignment of the image. **(E)** Air bubbles, formed inside the catheter, produce an attenuated image along the corresponding arc. Detail reveals the bubbles, bright structures, between 5 and 9 o’clock. **(F)** Fold over artifact (Fourier-domain optical coherence tomography system), the longitudinal view demonstrates that the cross section is located at the level of a side branch **(blue line)**.

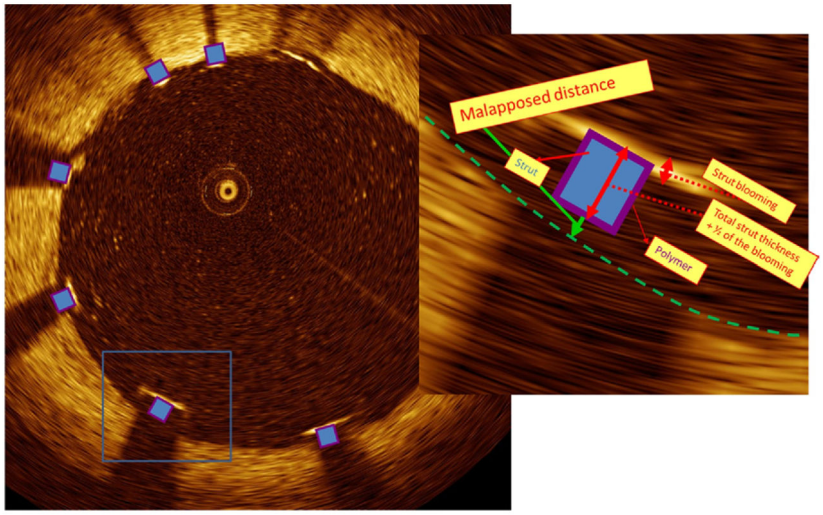

Figure 3. Malapposition Quantification

Cross-section image illustrating various levels of stent strut protrusion. Strut located at 7 o'clock is malapposed (detail). Malapposition is defined when the measured distance from the surface of the blooming to the lumen contour is higher than the total thickness of the stent strut + polymer + one-half of the blooming (the stent surface should be, theoretically, located at one-half the distance of the blooming thickness). In this particular case of a Taxus Express (Boston Scientific, Natick, Massachusetts) stent, the total, estimated, strut thickness = 164 μm (strut thickness = 132 μm + polymer = 16 μm + one-half of the blooming = 18 μm). The measured distance was 200 μm confirming a malapposed strut. Because of the eccentric wire position, the blooming component is elongated on the struts distant from the wire (5 and 7 o'clock), "merry-go-round" effect.

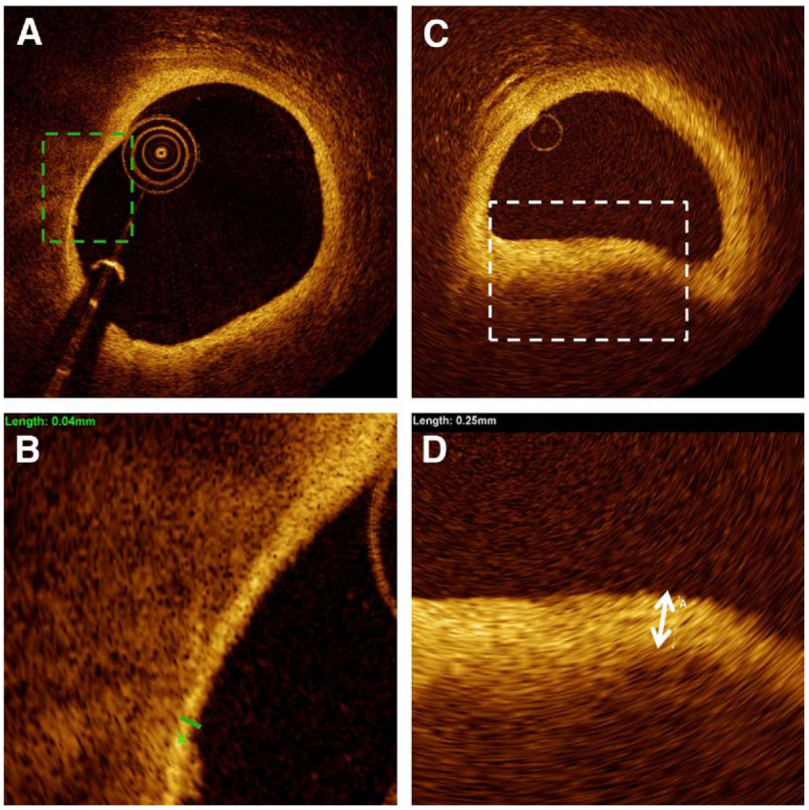

Figure 4. Fibrotic Cap Measurement

Representative cross section containing atherosclerotic plaque with different fibrotic cap thicknesses. **(A and B)** Thin fibrotic cap, measuring 40 μm. **(C and D)** Thick fibrotic cap, measuring 250 μm.

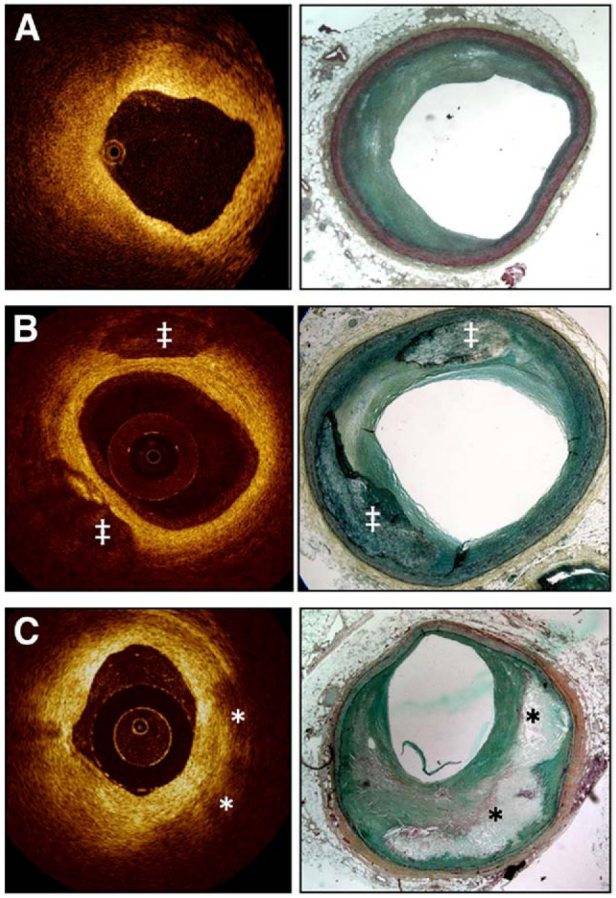

Figure 5. Optical Coherence Tomography: Histology Correlation

(A) Fibrotic plaque: characterized by high signal (high backscattering) and low attenuation (deep penetration). **(B)** Predominantly calcified plaque: calcified regions have a sharp border, low signal, and low attenuation permitting deeper penetration. **(C)** Lipid-rich plaque: the lipid core has a diffuse border. High light attenuation results in poor tissue penetration (in contrast to calcified regions). The overlying fibrotic cap can be readily measured; in this case a thick cap (>200 μm) is present. ‡Calcified region; *lipid core. Courtesy of LightLab Imaging (C. Y. Xu and J. M. Schmitt).

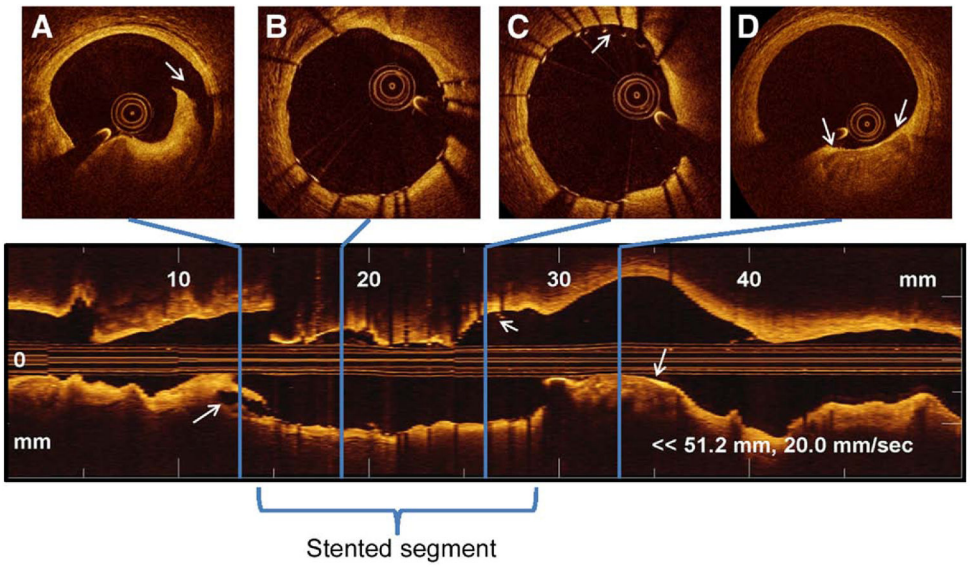

Figure 6. Coronary Imaging Acquired With an FD-OCT System

A longitudinal reconstruction **(lower panel)** and cross-sectional images **(upper panels)** acquired with a frequency or Fourier-domain optical coherence tomography (FD-OCT) system (Lightlab) at 20 mm/s immediately after stent implantation. Note that a 5-cm coronary segment was imaged with a 3-s contrast injection. **(A)** Distal edge dissection, with corresponding longitudinal view **(arrows). (B)** Well-expanded and well-apposed stent struts, with corresponding longitudinal view. **(C)** Malapposed struts between 11 and 1 o'clock, with corresponding longitudinal view **(arrows). (D)** Proximal calcified plaque with minimal fibrous coverage, with corresponding longitudinal view **(arrows)**.

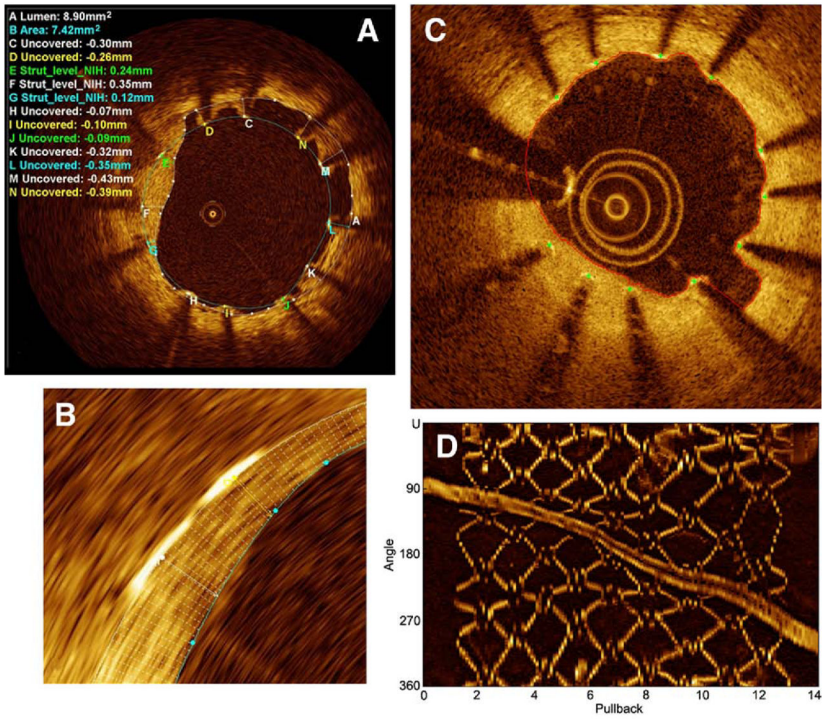

Figure 7. Quantitative Stent Analysis

(A) Representative frame depicting a Core-Lab area measurement and strut level analysis. Strut level analysis consists of a qualitative assessment for strut coverage and quantitative measurement from the surface of the blooming artifact to the lumen contour. A heterogeneity of strut coverage is observed within a single frame (C to N refer to labeled struts): covered struts (E to G), uncovered apposed struts (H to J), and malapposed struts (K to N, C and D). **(B)** Magnification of the automatic 360° chord system, applied between the stent and lumen contours, allowing a detailed measurement of the stent coverage. **(C)** Automatic lumen and stent detection: stent struts **(green dots)** and lumen contour **(red line). (D)** En face 3-dimensional view: the highly reflective stent surface allows easy discrimination of the struts from the surrounding tissue. **(C and D)** LightLab's automated stent strut analysis software (R&D program, not released) courtesy of LightLab Imaging (C. Y. Xu and J. M. Schmitt), images obtained at Wakayama University (Prof. Akasaka). NIH = neointimal hyperplasia.

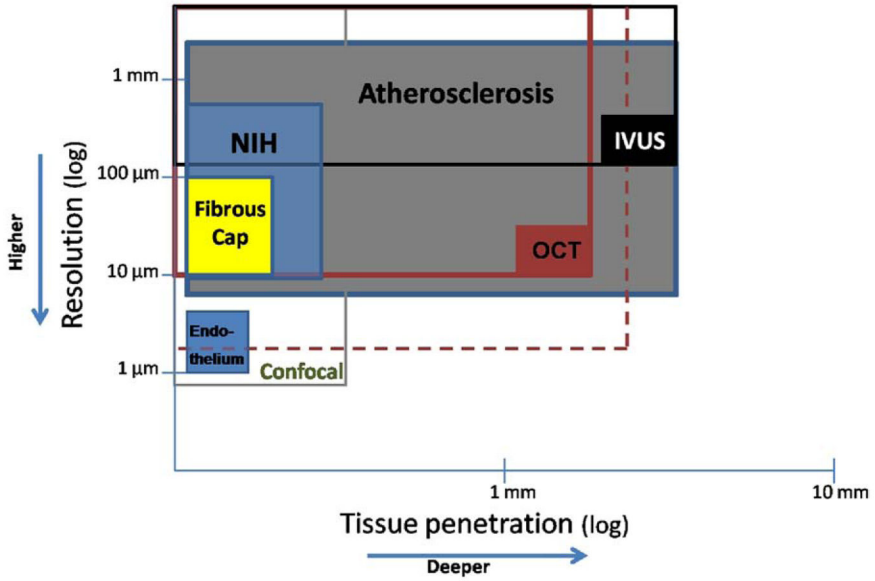

Figure 8. Comparison Between OCT Capabilities and Others' Imaging Methods

Graphic representation of tissue penetration versus spatial resolution of optical coherence tomography (OCT) compared with other imaging methods. The **solid boxes** represent the maximal resolution and depth achieved with current technologies. The larger **open boxes** represent the range of resolution and tissue penetration for each of the technologies. The **dashed box** illustrates the hypothetical capabilities of future OCT systems. Resolution requirements to accurately detect neointimal hyperplasia observed after drug-eluting stent (NIH) usually exceeds the capabilities of intravascular ultrasound (IVUS). Similarly, fibrous cap thickness can only be assessed in vivo by OCT. However, current OCT systems are not suitable to assess tissue at depths beyond 2 mm. Currently, evaluation of single cell endothelial layers can only be assessed in vitro by microscopy or advance bench-top OCT systems. Atherosclerosis = early and advanced stages of the process; Endothelium = single intimal cell layer; Fibrous Cap = thickness range related to thin cap fibroatheroma.

Table 1

Comparison Between TD-OCT and Prototype FD-OCT*

Specifications	TD-OCT	FD-OCT
Axial scans/s	5,000–10,000	~100,000
Lines/frame	~200	~500–1,000
Max. frame rate, fps	20	~200
Max. pullback speed, mm/s	3	20
Scan diameter (FOV), mm	6.8	~6–11
Axial resolution, μm	15	10–15
Lateral resolution, μm	90	20–40
Tissue penetration, mm	1.5–3	2–3.5
Balloon occlusion	Highly recommended	Optional
Catheter size, mm	0.48	0.8–1.0

*Values are approximate; TD-OCT specifications refer to the Lightlab time-domain optical coherence tomography (TD-OCT) system (M2/M3).

FD-OCT – frequency or Fourier-domain optical coherence tomography; FOV – field of view; TD-OCT – time-domain optical coherence tomography.

Table 2

General Characteristics of the Different Tissues by OCT

Tissue	Backscattering	Attenuation	General Aspects
Calcium	+	+	Sharp borders, low signal with heterogeneous regions
Lipid	++	+++	Irregular borders, superficial high signal followed by very low signal
Fibrotic	++	+	Homogeneous bright tissue
Red thrombus	+++	+++	Superficial signal rich, low penetration, signal-free shadowing
White thrombus	+++	+	Signal rich, more penetration than for red thrombus
Media layer	+	+	Low signal region, limited by 2 signal-rich band (IEL/EEL)
IEL/EEL	+++	+	High signal band (~20 μm)

IEL/EEL – internal elastic lamina/external elastic lamina; OCT = optical coherence tomography; + = low; ++ = moderate; +++ = high